

Lattice formulation of the Fokker-Planck equation

Simone Melchionna

INFN-SOFT, Department of Physics,

University of Rome “La Sapienza”, P.le A. Moro 2, 00185 Rome, Italy

Sauro Succi

Istituto per le Applicazioni del Calcolo “A. Picone”,

CNR, Viale del Policlinico 137, 00166, Roma, Italy

Jean-Pierre Hansen

Department of Chemistry, Lensfield Road,

Cambridge CB2 1EW, United Kingdom

Abstract

A lattice version of the Fokker-Planck equation (FPE), accounting for dissipative interactions, not resolved on the molecular scale, is introduced. The lattice FPE is applied to the study of electrorheological transport of a one-dimensional charged fluid, and found to yield quantitative agreement with a recent analytical solution. Future extensions, including inelastic ion-ion collisions, are also outlined.

I. INTRODUCTION

Over the last decade discrete lattice versions of kinetic equations, most notably the Lattice-Boltzmann (LB) method, have undergone burgeoning progress for the simulation of large scale hydrodynamic flows [1, 2, 3, 4] and of the dynamics of colloidal suspensions [5, 6]. The LB method was developed in response to major flaws of its predecessor, the lattice gas cellular automaton [7, 8], following the canonical route of classical Statistical Mechanics. A few years later the formal connection of the LB method with continuum kinetic theory was also elucidated [9].

One of the major appeals of the LB method is its flexibility, which allows to accommodate a host of complex physical effects, including boundary conditions at interfaces, intermolecular forces and even chemical reactions, through efficient and elegant discretizations of the force term in the kinetic Vlasov-Boltzmann equation. One of the limitations of the LB method is that, since it generates the time evolution of the one particle distribution function, fluctuations are not accounted for. “Brownian noise” becomes increasingly important as one explores flows on ever smaller scales, as in colloidal systems, or in narrow pores (microfluidics). The problem has been addressed on the colloidal scales, by incorporating a random (Brownian) force component in the momentum flux stress tensor [5, 10], or at the level of the discrete LB equation itself [6].

On the other hand, all LB implementations to date are based on the relaxation form of the collision operator, either in scalar [11] or tensorial form [12]. In this paper we show that the LB methodology can be easily extended to deal with small scale processes involving a Brownian component, by introducing a lattice version of the Fokker-Planck (FP) collision operator [13, 14]. In full analogy with the LB equation, the present lattice Fokker-Planck equation builds upon an optimized form of importance sampling of velocity space which, at variance with most numerical grid methods [14, 15, 16], permits to solve the Fokker-Planck equation near local-equilibrium in full single-particle phase space. The FP operator accounts for frictional dissipation due, e.g., to solute-solvent interactions or inelastic collisions with obstacles and confining surfaces, which need not be resolved on a molecular scale. We have, in particular, in mind electrorheological transport of ions confined in swollen clays, between membranes, or through water-filled nanopores (see e.g. [17]), like ion channels through membranes [18]. The FP equation has recently been applied to a detailed analysis

of stationary ion currents through one-dimensional pores of finite or infinite length [19], and analytic results were obtained in the case of independent (non-interacting) ions. In particular the ion current was shown to saturate with increasing applied field, and this result will serve as a benchmark for the numerical calculations presented later in this paper.

The paper is organized as follows. In section 2 we discuss the respective roles of the FP and Bhatnagar-Gross-Krook (BGK) collision operators in modelling transport and flows of solutes in implicit solvent and confined geometries. A one-dimensional kinetic model for ion transport through narrow pores is presented in Section 3. The lattice Fokker-Planck (LFP) equation for this problem is derived in Section 4. Numerical results are presented in Section 5 and compared to the predictions of ref. [19], while concluding remarks are made in Section 6. Stability analysis of the LFPE is outlined in the appendix.

II. FOKKER-PLANCK VERSUS BGK COLLISION OPERATORS

Kinetic equations for the time evolution of the distribution function $f(\mathbf{r}, \mathbf{v}; t)$ of a given species of particles conventionally involve a free-flow term (left-hand side) and a collision term (right-hand side), i.e.

$$(\partial_t + v_\alpha \partial_{x_\alpha} + a_\alpha \partial_{v_\alpha})f(\mathbf{r}, \mathbf{v}; t) = C[f(\mathbf{r}, \mathbf{v}; t)] \quad (1)$$

where x_α and v_α ($1 \leq \alpha \leq d$) are the cartesian components of the d-dimensional position and velocity vectors \mathbf{r} and \mathbf{v} , ∂_{x_α} and ∂_{v_α} are the components of the corresponding gradient operators, while $a_\alpha = F_\alpha/m$ are the components of the acceleration due to an externally applied, or a self-consistent force field \mathbf{F} (m is the particle mass). The Einstein convention of summation over repeated indices α is assumed. On the right hand side C denotes a collision operator (yet to be specified), acting on the distribution function f .

If one is interested in flows involving two (or more) species, e.g. a solvent and a solute, one may adopt one of two strategies:

a) one may treat the two species (say a and b) on the same footing, by introducing two distribution functions $f_i(\mathbf{r}, \mathbf{v}; t)$ ($i = a$ or b), associated with the two species, the time evolution of which is governed by two coupled kinetic equations. In the perspective of a discrete lattice formulation of the LB type, the simplest collision operators C_{ij} ($i, j = a$ or b) acting on the distribution functions are of the BGK form, involving several relaxation times

[20].

b) An alternative route, which is particularly appropriate when the solutes are colloidal particles, and which will be adopted here, is to assume a separation of time scales, and use an implicit solvent description of the Langevin form, involving frictional and random forces. The corresponding collision operator is the familiar Fokker-Planck operator [13, 14] which may also account for inelastic collisions of the solute particles with confining surfaces. In such an effective one-component description, the *dissipative* solute/solvent and solute/wall couplings are described by a FP collision operator, while *conservative* solute/solute collisions are described by a BGK operator. Explicitly, in the presence of the electric field,

$$(\partial_t + v_\alpha \partial_{x_\alpha} + a_\alpha \partial_{v_\alpha})f(\mathbf{r}, \mathbf{v}; t) = C^{FP}[f(\mathbf{r}, \mathbf{v}; t)] + C^{BGK}[f(\mathbf{r}, \mathbf{v}; t)] \quad (2)$$

where

$$C^{FP}[f] = \partial_{v_\alpha}(R_\alpha + D\partial_{v_\alpha})f \quad (3)$$

$$C^{BGK}[f] = -\omega(f - f_{BGK}^{eq}) \quad (4)$$

In eq. (3) R_α are the components of the drag force, which will be taken of the familiar form $\mathbf{R} = \gamma\mathbf{v}$, where γ is a constant friction coefficient, D characterizes diffusion in velocity space, and is related to γ by $D = \gamma v_T^2$, where $v_T = \sqrt{k_B T/m}$ is the thermal velocity and $\omega = 1/\tau$ is the solute-solute collision frequency.

The BGK collision operator entails a relaxation of the distribution function to the usual local Maxwellian equilibrium,

$$f_{BGK}^{eq}(\mathbf{r}, \mathbf{v}; t) = \frac{n(\mathbf{r}; t)}{(2\pi v_T^2)^{3/2}} e^{-(\mathbf{v}-\mathbf{u})^2/2v_T^2} \quad (5)$$

where $n(\mathbf{r}; t)$ is the local density, $\mathbf{u} = \mathbf{u}(\mathbf{r}; t)$ is the local average (or flow) velocity, while the thermal velocity v_T may depend on position and time, via the local temperature $T(\mathbf{r}; t)$.

The equilibrium resulting from the combined action of Fokker-Planck collisions and the electric field is given by a global shifted Maxwellian:

$$f_{FP,E}^{eq}(\mathbf{r}, \mathbf{v}; t) = \frac{n(\mathbf{r}; t)}{(2\pi v_T^2)^{3/2}} e^{-(\mathbf{v}-\mathbf{u}_E)^2/2v_T^2} \quad (6)$$

where $\mathbf{u}_E \equiv \frac{q\mathbf{E}}{m\gamma}$ is the drift speed associated with the electric field. By definition, the composite local equilibrium resulting from the competition of the two operators in the presence of an electric field satisfies the condition

$$C^{FP}[f^{eq}] + C^{BGK}[f^{eq}] - a_\alpha \partial_{v_\alpha} f^{eq} = 0 \quad (7)$$

This may be rewritten as

$$\mathcal{C}^{FP,E}[f^{eq}] = \frac{\omega}{\gamma}(f^{eq} - f_{BGK}^{eq}) \quad (8)$$

where $\mathcal{C}^{FP,E} = \partial_{v_\alpha}(v_\alpha + v_T^2 \partial_{v_\alpha}) - (a_\alpha/\gamma)\partial_{v_\alpha}$ is the Fokker-Planck operator including the electric field.

From the expression (8), it is clear that in the strongly dissipative regime $\omega/\gamma \rightarrow 0$, $f^{eq} \rightarrow f_{FP,E}^{eq}$, while the leading order correction is proportional to the difference $f_{FP,E}^{eq} - f_{BGK}^{eq}$, i.e. to the deviation of the local flow field \mathbf{u} from the drift speed \mathbf{u}_E . This is consistent with the fact that when $\mathbf{u} = \mathbf{u}_E$, a condition which is reached at steady-state, the FP and BGK equilibria coincide.

The interplay between the FP and BGK collision operators spawns a rich variety of physical effects, which will be the object of future investigations. In the sequel, however, we shall confine our attention to the methodological aspects related to the lattice formulation of the Fokker-Planck equation. For illustration purposes, and the sake of simplicity, we henceforth restrict the discussion to the case $d = 1$ (one spatial dimension) of the FP equation and to its validation by comparison with recent exact results.

III. A ONE-DIMENSIONAL KINETIC MODEL FOR TRANSPORT THROUGH PORES

In this Section the implicit solvent kinetic model introduced in the previous Section is applied to the important problem of single-file ion transport through a water-filled pore connecting two reservoirs, under the action of an applied electric field or ion-concentration gradient. The one-dimensional version of the kinetic model (2)-(4) provides a crude representation of ion permeation of ion channels through membranes separating intra and extra-cellular compartments [18, 19]. Ion permeation of such channels has been examined by numerous Molecular Dynamics (MD) or Brownian Dynamics (BD) simulations of realistic or semi-realistic quasi-cylindrical models (for a review, see [21]) or by numerical solutions of the Poisson-Nernst-Planck equations [22], but the present study is inspired by the recent kinetic modelling of ref. [19].

The action of the confining, quasi-cylindrical pore is crudely represented by restricting ion motion to one dimension and by a contribution to the frictional force $-\gamma v$.

The one-dimensional version of the kinetic equation (2)-(4) may be cast in the form

$$(\partial_t + v\partial_x)f = C^{FP}[f] + C^{BGK}[f] - a\partial_v f = \partial_v[\gamma(vf + v_T^2\partial_v f)] - \omega(f - f_{BGK}^{eq}) - a\partial_v f \quad (9)$$

where $f = f(x, v; t)$ and $a = qE/m$, E being the applied electric field and q the charge of the ions; in practice one is mostly interested in mono or divalent cations ($q = +e$ or $+2e$). The last two terms on the r.h.s. of eq. (9) may be regrouped into a single FP-like term

$$C^{FP}[f] - a\partial_v f = \partial_v\gamma[(v - u_E)f + v_T^2\partial_v f] \quad (10)$$

where $u_E = qE/m\gamma = a/\gamma$ is the ion drift velocity in response to the applied field.

The local equilibrium solution of the kinetic equation (9) is hence

$$f_{BGK}^{eq}(x, v; t) = \frac{n(x; t)}{(2\pi v_T^2)^{1/2}} e^{-[v - u(x; t)]^2/2v_T^2} \quad (11)$$

The zeroth, first and second moments of the distribution are the local density n , current J and pressure (or momentum flux) P per unit mass

$$n(x; t) = \int_{-\infty}^{\infty} f(x, v; t) dv \quad (12)$$

$$J(x; t) = \int_{-\infty}^{\infty} v f(x, v; t) dv \equiv n(x; t)u(x; t) \quad (13)$$

$$P(x; t) = \int_{-\infty}^{\infty} v v f(x, v; t) dv \quad (14)$$

Note that in one dimension the momentum flux is proportional to the (kinetic) energy, but this is of course no longer true in higher dimension.

By multiplying both sides of the kinetic equation (9) successively by 1, v and v^2 , and integrating over all v , one easily arrives at the following macroscopic equations

$$\partial_t n(x; t) + \partial_x J(x; t) = 0 \quad (15)$$

$$\partial_t J(x; t) + \partial_x P(x; t) = -\gamma J(x; t) + n(x; t)a \quad (16)$$

$$\partial_t P(x; t) + \partial_x Q(x; t) = -2\gamma n(x; t)\frac{u^2(x; t)}{2} + 2aJ(x; t) \quad (17)$$

Eq.(15) is the continuity equation expressing the conservation of mass; equation (16) expresses momentum balance with proper account of friction and acceleration due to the electric field while (17) is the energy balance equation, taking into account the heat flux

$$Q(x; t) = \int_{-\infty}^{\infty} v^2 v f(x, v; t) dv \quad (18)$$

as well as frictional dissipation. The standard kinetic equation with the BGK collision operator yields the same three macroscopic equations without the dissipative contributions stemming from the FP collision operator. In the case of a steady, homogeneous flow, eq.(16) leads back to Ohm's law, $qJ = \sigma E$, with a conductivity $\sigma = nq^2/\gamma m$.

Stationary solutions of eq. (9) have been obtained in the case of independent ions ($\omega = 0$), for finite length as well as infinitely long channels in ref. [19]. Solutions in the non-stationary case, and including the BGK collision term in addition to the FP term, can only be obtained numerically. In the next section we derive the lattice version of the kinetic equation (9).

IV. THE LATTICE-FOKKER-PLANCK EQUATION

The lattice version of the kinetic equation (9) may be systematically derived along the lines leading to the LB equation[23]. Since the latter is well documented[1, 2, 3, 4] we restrict most of the following discussion to the FP collision operator (10).

The distribution function is expanded onto a Hermite basis

$$f(x, v; t) = \sum_{k=0}^K F_k(x; t) h_k(v) w(v) \quad (19)$$

where $w(v) = (2\pi v_T^2)^{-1/2} e^{-v^2/2v_T^2}$ is the one-dimensional Hermite weight function, while $h_k(v)$ is the Hermite polynomial of order k . By substituting eq.(19) into the kinetic equation eq.(9), and projecting upon the Hermite basis, one arrives at

$$\partial_t F_l(x; t) + \partial_x G_l(x; t) = C_l(x; t) \quad (20)$$

where

$$F_l(x; t) = \int_{-\infty}^{\infty} f(x, v; t) h_l(v) dv \quad (21)$$

$$G_l(x; t) = \int_{-\infty}^{\infty} v f(x, v; t) h_l(v) dv \quad (22)$$

$$C_l(x; t) = \int_{-\infty}^{\infty} C^{FP}[f(x, v; t)] h_l(v) dv \quad (23)$$

C^{FP} being the linear FP operator (10).

Equations (20) are the usual moment relations associated with the FP equations. The next step is to evaluate the kinetic moments F_l , G_l and C_l by Gauss-Hermite quadrature. Noting that $f(x, v; t)/w(v)$ is a polynomial in v , the quadrature reads

$$F_l(x; t) = \sum_{i=0}^{G-1} \frac{f(x, v_i; t)}{w(v_i)} w_i h_l(v_i) \quad (24)$$

where the v_i and w_i are the nodes and weights of the quadrature. It is crucial to observe that Eq. (24) is exact for polynomials of degree up to $(2G + 1)$. This means that the present Hermite-Gauss projection is *de-facto* equivalent to an optimized form of importance sampling of velocity space. It is this discretization which permits to compute the evolution of the low-order macroscopic moments (density-current) more efficiently than any standard discretization of velocity space (see ref. [15] and references therein). In fact, any grid method would necessarily use a mesh-spacing in velocity space which is a fraction, say at most $1/10$, of the thermal speed, v_T . Covering a few units of v_T would then take at least 30-50 grid points in velocity space. In contrast, LFPE only needs at most five. The advantage to LFPE would be even more substantial in higher dimensions.

Expressions similar to Eq.(24) hold for G_l and C_l . Substituting these into eq. (20), and identifying the factors of $h_l(v_i)$ on both sides of the resulting sum, one obtains the following set of equations

$$\partial_t f_i(x; t) + v_i \partial_x f_i(x; t) = c_i(x; t) \quad 0 \leq i \leq G - 1 \quad (25)$$

where the following identifications have been made

$$f_i(x; t) \equiv \frac{f(x, v_i; t) w_i}{w(v_i)} \quad (26)$$

$$c_i(x; t) \equiv \frac{C^{FP}[f(x, v_i; t)] w_i}{w(v_i)} \quad (27)$$

The discrete collision operator is entirely specified by the coefficients c_i defined by eq. (27). These can be unambiguously computed from the spectral decomposition of the continuous operator $C^{FP}[f(x, v; t)]$ similar to eq. (19), i.e.

$$C^{FP}(v_i) \equiv C^{FP}[f(x, v_i; t)] = \sum_{k=0}^K C_k(x; t) h_k(v_i) w(v_i) \quad (28)$$

Knowledge of the spectral coefficients $C_k(x, t)$ allows the discrete coefficients $c_i(x; t)$ in eq.(27) to be calculated, thereby providing an operational definition of the discrete FP operator.

The last step is to perform time integration along the characteristics $dx_i = v_i dt$ according to the standard practice of LB algorithms. This yields the desired lattice-Fokker-Planck (LFP) equation

$$f_i(x + v_i \Delta t, t + \Delta t) - f_i(x, t) = c_i(x; t) \Delta t \quad (29)$$

where Δt is the time-step chosen for the numerical solution.

The spectral coefficients of the FP operator are easily calculated to be

$$C_0 = 0 \quad (30)$$

$$C_1 = -\gamma J + na \quad (31)$$

$$C_2 = -2\gamma(P - nv_T^2) + 2aJ \quad (32)$$

$$C_3 = -3\gamma(Q - 3v_T^2 J) + 3a(P - nv_T^2) \quad (33)$$

$$C_4 = -4\gamma(R - 5v_T^2 P + 2nv_T^4) + 4a(Q - 2Jv_T^2) \quad (34)$$

where $R = \int_{-\infty}^{\infty} dv v^4 f(x, v; t)$ and the first four Hermite polynomials are $h_0 = 1$, $h_1 = v$, $h_2 = v^2 - v_T^2$, $h_3 = v^3 - 3vv_T^2$, $h_4 = v^4 - 4v^2 v_T^2 + v_T^4$. High order coefficients (C_k ; $k \geq 2$) differ from those derived from the BGK operator (if $\omega = \gamma$). All coefficients, as well as n , u , P and Q , defined by eqs (12)-(14) and (18), and R , are local quantities, depending on x and t .

Returning to the LFP equation (29), we now consider two discretized models, namely Q_3 and Q_5 , involving three and five velocities and where $v_T^2 = 1/3$ and $v_T^2 = 1$ respectively. Within Q_3 the velocities v_i and associated weights w_i are

$$\begin{aligned} v_0 &= 0 & w_0 &= 2/3 \\ v_1 &= +1; & w_1 &= 1/6 \\ v_2 &= -1; & w_2 &= 1/6 \end{aligned} \quad (35)$$

The three velocities v_i ($i = 0, 1, 2$) may be considered as the components of a three-vector $(0, 1, -1)$. It proves convenient to construct a basis of three such vectors $\mathbf{A}^{(k)}$ which satisfy the orthonormality conditions

$$\mathbf{A}^{(k)} \cdot \mathbf{A}^{(l)} = \sum_{i=0}^2 A_i^{(k)} A_i^{(l)} w_i = \delta^{(k,l)} \quad (36)$$

These vectors are easily calculated to be

$$\begin{aligned} \mathbf{A}^{(0)} &= (1, 1, 1) \\ \mathbf{A}^{(1)} &= \sqrt{3}(v_0, v_1, v_2) = \sqrt{3}(0, 1, -1) \\ \mathbf{A}^{(2)} &= \frac{3}{\sqrt{2}}(v_0^2 - v_T^2, v_1^2 - v_T^2, v_2^2 - v_T^2) = \frac{1}{\sqrt{2}}(-1, 2, 2) \end{aligned} \quad (37)$$

within this basis, the collision operator in eq. (29) may be cast in the form

$$c_i(x, t) = (C_0 A_i^{(0)} + C_1 A_i^{(1)} + C_2 A_i^{(2)}) w_i \quad (38)$$

The various x and t -dependent quantities follow from the definitions (12)-(14) by replacing the integrals over velocities by sums over the 3 discrete velocities v_0 , v_1 and v_2 , using the proper weights w_i . These prescriptions entirely specify the Lattice Fokker-Planck (LFP) equation for the model Q_3 . The same procedure may be used to specify the LFP equation for the Q_5 model, where the 5 velocities are $(-2, -1, 0, 1, 2)$, and the corresponding weights w_i are $(1/12, 1/6, 1/2, 1/6, 1/12)$, with a resulting thermal speed $v_T = 1$.

The Lattice BGK equation has been widely described in the literature [3], and therefore only a very sketchy description is provided below. The lattice BGK equation has the same form as eq.(29), where the lattice BGK collision operator is given by

$$c_i^{BGK} = -\omega(f_i - f_{BGK,i}^{eq}) \quad (39)$$

The local equilibrium takes the form of a local Maxwellian expanded to second order in the Mach number $M = u/v_T$,

$$f_{BGK,i}^{eq} = w_i n \left(1 + \frac{v_i u}{v_T^2} + \frac{(v_i v_i - v_T^2) u^2}{2v_T^4} \right) \quad (40)$$

The lattice equilibria, including the weights w_i , are designed on the requirement of fulfilling mass and momentum conservation, that is

$$\sum_{i=0}^{G-1} f_{BGK,i}^{eq} = \sum_{i=0}^{G-1} f_i = n \quad (41)$$

and

$$\sum_{i=0}^{G-1} f_{BGK,i}^{eq} v_i = \sum_{i=0}^{G-1} f_i v_i = nu \quad (42)$$

The parameter ω is an inverse relaxation scale which controls the shear viscosity of the lattice fluid.

V. NUMERICAL RESULTS

As a first application and test of the LFP formalism, we consider the single-file transport of ions through a pore of length L connecting two reservoirs containing ions at given

concentrations. As in ref. [19] we assume that at both ends of the pore, the ion distribution function is a Maxwell-Boltzmann equilibrium distribution at temperature T which determines the thermal velocity v_T . For instance, in the Q_3 case, boundary conditions are imposed as follows

$$\begin{aligned} f_1(x=0, t) &= \frac{n_l}{\sqrt{2\pi}} \\ f_2(x=L+1, t) &= \frac{n_r}{\sqrt{2\pi}} \end{aligned} \quad (43)$$

where subscripts 1 and 2 stand for rightward and leftward propagation and n_l , n_r indicate the left and right reservoir densities respectively. The reservoirs are located at $x=0$ and $x=L+1$ respectively, while the physical channel runs from $1 \leq x \leq L$. Note that the expressions (43) correspond to fixing the incoming *fluxes* from the reservoirs, hence they do not imply that n_l and n_r coincide with the fluid density at inlet and outlet sections. In fact, since the ion distribution function in the reservoirs is a Maxwellian at zero macroscopic speed, continuity of the fluxes (current density), implies a discontinuity of both density and velocity profiles at both ends of the channel.

We define the dimensionless current

$$J^* = J \sqrt{\frac{2\pi}{v_T^2}} \frac{1}{n} \quad (44)$$

the dimensionless acceleration, or electric field

$$a^* = \frac{maL}{k_B T} = \frac{qEL}{k_B T} = \frac{E}{E_T} \quad (45)$$

and the dimensionless collision rate

$$\gamma^* = \frac{\gamma L}{v_T} = \frac{\gamma}{\gamma_T} = \frac{E_\gamma}{E_T} \quad (46)$$

where n is the reservoir ion density, $E_T = k_B T/qL$ is a “thermal” electric field, such that the work it produces to move a charge q over the channel length L equals the thermal energy $k_B T$, while $E_\gamma = \gamma k_B T/(qv_T) = m\gamma v_T/q$ is the electric field producing on a charge q a force which balances the frictional force $-m\gamma v_T$. In other words, in a linear regime, the drift velocities associated with E_T and E_γ are $u_T = v_T/\gamma^*$ and $u_\gamma = v_T$ respectively. Clearly, in infinitely long channels, or zero-temperature fluids, $u_T \rightarrow 0$, and the ionic current is controlled by pure dissipation, $u_E = \frac{qE}{m\gamma}$. In finite-size, finite-temperature situations, and

constant-flux boundary conditions, however, deviations from this simple Ohmic regime must be expected, as we shall show in the sequel.

We have solved the LFP equation numerically to determine the stationary distribution function $f(x, v)$ and derive the corresponding macroscopic moments, primarily the current $J(x)$. Since we focus on the Fokker-Planck operator, for the time being, we exclude ion-ion collisions by setting $\omega = 0$.

In Figure 1, the stationary density profiles $n(x)$ calculated with the Q_3 and Q_5 models for two values of the electric field, $a^* = 1$ (moderate) and $a^* = 3$ (strong), are compared to the analytical result of the continuous velocity model [19], which reads as follows:

$$n_{exact}(x) = Ae^{a^*x/L} + B$$

where

$$A = \frac{1}{2 \sinh(a^*/2)} \left[n_r - n_l + \frac{a}{a^*} \sqrt{2\pi} B \right]$$

$$B = \frac{n_l e^{a^*/2} - n_r e^{-a^*/2}}{2 \sinh(a^*/2) e^{-a^{*2}/2\gamma^{*2}} + \sqrt{\frac{\pi}{2}} \frac{a^*}{\gamma^*} \left[\cosh(a^*/2) + \sinh(a^*/2) \int_{-v_T a^*/\gamma^*}^{v_T a^*/\gamma^*} dv \Phi(v) \right]}$$

and $\Phi = \sqrt{1/2\pi v_T} \exp(-v^2/2v_T^2)$. The total current flowing through the channel is $J_{exact} = aB/\gamma$. It should be appreciated that the strongly non-linear dependence of the current (see the expression of B) reflects the highly non-trivial competition between the effect of the boundary conditions and the electric field.

The ratio of the numerical to analytical density profiles $n(x)/n_{exact}(x)$, is seen to deviate from the unit value of about 10% for $a^* = 3$ and less than 5% for $a^* = 1$. These departures can be attributed to the constant-flux boundary conditions which, as discussed previously, introduce a discontinuity at the open ends of the channel. We also notice that the Q_5 solution appears appreciably more accurate than the Q_3 one. At lower values of the electric field, both Q_3 and Q_5 yield excellent agreement with the analytical solution.

The current-voltage relation is illustrated in Fig. 2, where the reduced current J^* is plotted as a function of the reduced electric field, $a^* \equiv E/E_T$, for three values of the reduced collision rate $\gamma^* = E_\gamma/E_T = 1, 5, 10$. Results obtained with the Q_3 and Q_5 models are compared to the analytical predictions of ref. [19], where the problem was solved for a continuous velocity spectrum (Q_∞). First, we notice that the Ohmic regime, $E/E_T \ll 1$,

is well reproduced in all three cases. As the strength of the electric field is increased, the current shows the saturation effect predicted by the analytical results [19].

This saturation is a direct consequence of the imposed boundary conditions. Since the reservoirs cannot feed more than nv_T ions per unit area and time, the current cannot exceed its ballistic value $v_T n / \sqrt{2\pi}$ in the limit $E \rightarrow \infty$. The rate of convergence towards the asymptotic limit depends sensitively on the reduced collision rate γ^* . Fig. 2 shows that the results obtained with the Q_5 model are systematically closer to the exact results than those obtained with the Q_3 model.

We have also checked that with simple boundary conditions, e.g. periodic, Ohm's law $J^* = E^* / \gamma^*$, is reproduced to machine accuracy and independently on the grid size, beyond about 100 grid points. However, the present case is much more challenging due to the highly non-trivial boundary conditions. In fact, a very slow convergence of the results as a function of grid resolution is observed (see Figure 3). This is probably caused by the representation of the reservoirs by a single lattice point without making allowance for any finite size transition region between the current-carrying distribution function in the channel and the no-current equilibrium current in the reservoirs. The consequence of a less abrupt treatment of the boundaries will be explored in the future.

VI. EFFECTS OF ION-ION COLLISIONS

The BGK collision operator (39) does not make any contribution to the continuity and momentum equations because, by construction, ion-ion collisions have been designed to conserve mass and momentum (elastic collisions). As a result, the BGK operator does not contribute to the momentum equation, and consequently, it cannot produce any effect on the electric conductivity of the system. In fact, ion-ion collisions are in control of the shear viscosity of the charged fluid, clearly an irrelevant notion in one-dimensional systems.

However, in electro-rheological flows, ions move in the presence of a surrounding solvent, typically water. It is therefore reasonable to assume that ion-ion "effective" collisions may become inelastic on account of the ion interaction with the solvent. A natural way to include such inelastic effects within the BGK operator is to assume a mismatch between the equilibrium current $J^{eq} = \sum_{i=0}^{G-1} f_i^{eq} v_i$ and the actual current J carried by the ions. The

simplest form for such a mismatch is

$$J^{eq} = \lambda J \quad (47)$$

where λ is a parameter measuring the degree of inelasticity of the 'effective' ion-ion collisions ($0 < \lambda < 1$ for passive solvents, i.e. momentum absorbing media, while $\lambda > 1$ denotes active solvents, i.e. momentum-imparting media, and $\lambda = 1$ for standard elastic collisions).

The relation (47) is readily implemented by replacing u with λu in the second term within parentheses on the right hand side of the eq. (40). With this modification, the BGK collision operator contributes a term $-\omega(J - J^{eq}) = -\omega(1 - \lambda)J$ to the momentum equation, so that inelastic collisions make themselves felt through an effective frequency $\omega_\lambda = (1 - \lambda)\omega$. As a result, setting aside boundary conditions, i.e. in an infinitely long channel, for simplicity, the steady-state current is given by

$$J = \frac{nE/\gamma}{1 + \omega_\lambda/\gamma}$$

This expression has been checked against numerical simulations (with periodic boundary conditions) for $\lambda = 0$ (fully inelastic) and $\lambda = 1$ (fully elastic), with $\gamma = 0.1$ and $\omega/\gamma = 0.1, 1, 10$. In Figure 4, we report the ratio $J(\lambda = 0)/J(\lambda = 1)$ as a function of the electric field strength, and compare it with the analytical result $\gamma/(\gamma + \omega)$. From this figure, excellent agreement with the analytical results is clearly appreciated. Although the present test only serves the purpose of illustrating the basic idea, it is hoped that combination of the lattice Fokker-Planck equation with inelastic BGK operators, will permit to explore complex situations in one, two and three dimensions, out of reach of analytical methods, such as multicomponent fluids (ions, cations and solvent) with heterogeneous surface interactions, trapping effects and related phenomena.

VII. CONCLUSION

In conclusion, we have developed a lattice version of the Fokker-Planck equation (FPE) which, by construction, can solve near-equilibrium kinetic problems in the full single-particle phase space. The main scope of the lattice FPE is to account for dissipative interactions not resolved at the molecular scale, such as fluid interactions with solid walls and/or solute-solvent collisions. The lattice FPE has been applied to the study of electrorheological transport of a one-dimensional charged fluid, and found to yield satisfactory agreement with a

recent non-trivial analytical solution, especially for the five-speed case. In particular, the lattice FPE proves capable of predicting the saturation effect resulting from the non-linear interaction between the electric field and the constant-flux boundary conditions imposed by the presence of equilibrium reservoirs at the channel boundaries.

The present lattice FPE extends straightforwardly to higher dimensions and it might prove useful for the numerical investigation of more complex situations, such as heterogeneous channels with kinetic traps, and/or multicomponent fluids, for which analytical solutions are no longer available.

Acknowledgments

JPH acknowledges the generous support of INFM while in Rome and the kind hospitality of G. Ciccotti and G. Parisi. The authors are grateful to D.Moroni, B. Rotenberg and A. Louis for useful comments and discussions.

Appendix A: STABILITY ANALYSIS OF THE LATTICE FPE

Being derived from the same principles, the lattice Fokker-Planck equation shares many features with the Lattice Boltzmann equation. Among the main advantages: i) a very efficient sampling of velocity space, which permits to work in steps of size $\Delta v = v_T$ rather than of a fraction thereof; ii) since the discrete speeds v_i are constant, the streaming operator $v\partial_x f$ can be integrated *exactly* along the characteristics $\Delta x = v_i\Delta t$, i.e. by a mere shift of the discrete distribution from site x to site $x + v_i\Delta t$, iii) the collision operator is completely local in space, which makes the Lattice FPE well suited to parallel computing. Of course, there are limitations too. In particular, the damping rate is approximately bounded within the range

$$a/v_T < \gamma < 1/\Delta t$$

The lower bound relates to the fact that damping rates below a/v_T imply that particles may acquire a drift speed $u = a/\gamma$ larger than the thermal speed. This endangers the stability of the lattice FPE, because the condition $u > v_T$ may violate the positive-definiteness of the truncated distribution (eq.19), which consists only of a very limited number of Hermite polynomials. Thus, in full analogy with LBE, the lattice FPE is best suited to describe near-

equilibrium, low-Mach number flows, with $u/v_T \ll 1$. The upper boundary is dictated by a stability condition of the time-marching scheme, specifically of the explicit time integration of the collision operator (we recall that the streaming operator is integrated exactly). The stability of the lattice FPE can be estimated by means of the following inequality

$$\left| \frac{C_k \Delta t}{F_k} \right| < 1 \quad (\text{A1})$$

which states that the change in the macroscopic moment $F_k(x, t)$ due to collisions in a time step Δt , should not exceed the value of $F_k(x, t)$ itself.

In order to elaborate this condition further, we recall the expression of the five Hermite polynomials relevant to the Q_5 lattice, that is:

$$\begin{aligned} h_0(v_i) &= 1_i = [1, 1, 1, 1, 1] \\ h_1(v_i) &= v_i = [-2, -1, 0, +1, +2] \\ h_2(v_i) &= v_i^2 - v_T^2 = [3, 0, -1, 0, 3] \\ h_3(v_i) &= v_i^3 - 3v_T^2 v_i = [-2, 2, 0, -2, 2] \\ h_4(v_i) &= v_i^4 - 4v_T^2 v_i^2 + v_T^4 = [1, -2, 1, -2, 1] \end{aligned}$$

The corresponding macroscopic moments in equations (30)-(34), are given by:

$$F_0 = n \quad (\text{A2})$$

$$F_1 = J \quad (\text{A3})$$

$$F_2 = nu^2 \quad (\text{A4})$$

$$F_3 = Q - 3Jv_T^2 \quad (\text{A5})$$

$$F_4 = R - 4nv_T^2 u^2 - 3nv_T^4 \quad (\text{A6})$$

In view of these expressions, the stability condition (A1) is readily recast in a more informative form as:

$$k\gamma\Delta t < 1, \quad k = 1, 4 \quad (\text{A7})$$

A more specific result can be obtained by analyzing the dispersion relation associated with the lattice FPE. Upon Fourier-transforming the lattice FPE eq.(29), $f_i(x, t) = \sum_{k, \omega} f_i(k, \omega) e^{I(kx - \omega t)}$, we obtain (I denotes the imaginary unit):

$$\sum_j [(e^{-I(\omega - kv_i)\Delta t} - 1)\delta_{ij} - C_{ij}\Delta t] f_j = 0 \quad (\text{A8})$$

where C_{ij} is the collision matrix associated with the Fokker-Planck operator. This matrix can be computed as follows. Consider the definition of the spectral coefficient C_l in eq.(23), and express the function $C^{FP}[f]$ as $\hat{C}f$, where $\hat{C} = \partial_{v_\alpha}[R_\alpha + D\partial_{v_\alpha}]$ is the Fokker-Planck operator acting upon $f(x, v, t)$. By expanding the function f on the Hermite basis as given by eq.(19), eq.(23) takes the form

$$C_k = \sum_l C_{kl} F_l \quad (\text{A9})$$

where

$$C_{kl} = \int h_k(v) \hat{C} w(v) h_l(v) dv \quad (\text{A10})$$

is the matrix representation of the Fokker-Planck operator in the global Hermite basis. By using eq.(24) to express F_l in terms of f_j , we obtain:

$$C_i = \sum_{kl} C_{kl} h_k(v_i) w_i \sum_j h_l(v_j) f_j \equiv \sum_j C_{ij} f_j$$

which defines the collision matrix C_{ij} as:

$$C_{ij} = w_i \sum_{kl} h_k(v_i) C_{kl} h_l(v_j) \quad (\text{A11})$$

The above expression is the operational key of the lattice FPE and lends itself to a fairly transparent physical interpretation. The matrix element C_{ij} , expressing the effect of population f_i on population f_j , is a weighted average over all spectral modes, the weights being the Hermite eigenfunctions evaluated at $v = v_i$ and $v = v_j$ respectively.

It is now convenient to normalize the Hermite coefficients $h_k(v_i)$ as follows:

$$h_{ik} \equiv h_k(v_i) / \sqrt{H_k}$$

where $H_k = \sum_i h_k(v_i) w_i h_k(v_i)$ are the normalization factors, explicitly $H_0 = 1, H_1 = 1, H_2 = 2, H_3 = 2, H_4 = 2$.

The expressions (A11) and (A10) are nothing but the matrix representations of the Fokker-Planck operator in the local (Dirac's deltas) and global (Hermite polynomials) basis functions. The transformation between these two representations is performed by the matrix h_{ik} . It is readily checked that this matrix fulfills the orthonormality condition

$$\sum_k h_{ik} w_i h_{kj} = \delta_{ij}$$

Consequently, the matrices C_{ij} and C_{kl} are related by a similarity transformation, hence they are iso-spectral (they share the same eigenvalues).

The spectrum of C_{kl} can be obtained by direct inspection of eq.s (30)-(34) for the case $E = 0$, and taking into account the definitions (A2). The resulting matrix C_{kl} is identified as:

$$C_{kl} = \begin{pmatrix} 0 & 0 & 0 & 0 & 0 \\ 0 & -\gamma & 0 & 0 & 0 \\ 0 & 0 & -2\gamma & 0 & 0 \\ 0 & 0 & 0 & -3\gamma & 0 \\ 0 & 0 & 4\gamma & 0 & -4\gamma \end{pmatrix}$$

which delivers the following five eigenvalues:

$$\lambda_k = -k\gamma, \quad k = 0, 4$$

Note the zero eigenvalue associated with mass conservation.

According to standard arguments of Lattice Boltzmann theory [1], the stability condition associated with the dispersion relation (A8), reads as follows:

$$|1 - k\gamma\Delta t| < 1, \quad k = 1, 4 \tag{A12}$$

This is satisfied within the range

$$0 < \gamma\Delta t < 1/2 \tag{A13}$$

It is perhaps interesting to observe that the procedure outlined in this Appendix can be applied to a very broad class of kinetic equations, including the Klein-Gordon and Schrödinger equations of quantum mechanics [24].

-
- [1] R. Benzi, S. Succi, and M. Vergassola, *Phys.Reports* **222**, 145 (1992).
 - [2] D. Wolf-Gladrow, *Lattice Gas Cellular Automata and Lattice Boltzmann Models* (Springer Verlag, Berlin, 2000).
 - [3] S. Succi, *The Lattice Boltzmann Equation for Fluid Dynamics and Beyond* (Oxford University Press, Oxford, 2001).
 - [4] S. Chen and G. D. Doolen, *Annu. Rev. Fluid Mech.* **30**, 329 (1998).
 - [5] A. Ladd and R. Verberg, *J. Stat. Phys.* **104**, 1191 (2001).
 - [6] M. Cates *et al.*, *J. Phys. Condens. Matter* **16**, S3903 (2004).

- [7] U. Frish, B. Hasslacher, and Y. Pomeau, Phys. Rev. Lett. **56**, 1505 (1986).
- [8] B. Eu, *Kinetic Theory and Irreversible Thermodynamics* (Wiley, New York, 1992).
- [9] X. Shan and X. He, Phys. Rev. Lett. **80**, 65 (1998).
- [10] A. Ladd, Phys. Rev. Lett. **70**, 1339 (1993).
- [11] P. Bhatnagar, E. Gross, and M. Krook, Phys. Rev. **94**, 511 (1954).
- [12] F. Higuera, S. Succi, and R. Benzi, Europhys. Lett. **9**, 345 (1989).
- [13] N. van Kampen, *Stochastic Processes in Physics and Chemistry* (North Holland, Amsterdam, 1981).
- [14] H. Risken, *The Fokker-Planck Equation* (Springer Verlag (2nd ed.), Berlin, 1989).
- [15] D. Zhang, G. Wei, D. Kouri, and D.K.Hoffman, Phys. Rev. E **56**, 1197 (1997).
- [16] J. Fok, B. Guo, and T. Tang, Math. Comp. **71**, 1497 (2002).
- [17] S. Melchionna and S. Succi, J. Chem. Phys. **120**, 4492 (2004).
- [18] B. Hille, *Ionic Channels of Excitable Membranes* (Sinauer Associated (2nd ed.), Sunderland, MD, 1992).
- [19] J. Piasecki, R. Allen, and J.-P. Hansen, Phys. Rev. E **70**, 021105 (2004).
- [20] L. Luo and S. Girimaji, Phys. Rev. E **67**, 036302 (2003).
- [21] D. Tieleman, P. Biggins, G. Smith, and M. Sansom, Quart. Rev. Biophys. **44**, 473 (2001).
- [22] D. Chen and R. Eisenberg, Biophys. J. **64**, 1405 (1993).
- [23] X. Shen, and X. He, Phys. Rev. Lett., **80**, 65 (1998).
- [24] S. Succi and R. Benzi, Physica D **69**, 327 (1993).

Figure 1: Ratio of numerical to analytical density profiles along a channel of length 10000, for $a^* = 1.0$ and $a^* = 3.0$. The solid line and the dashed line correspond to the Q_3 and the Q_5 models respectively.

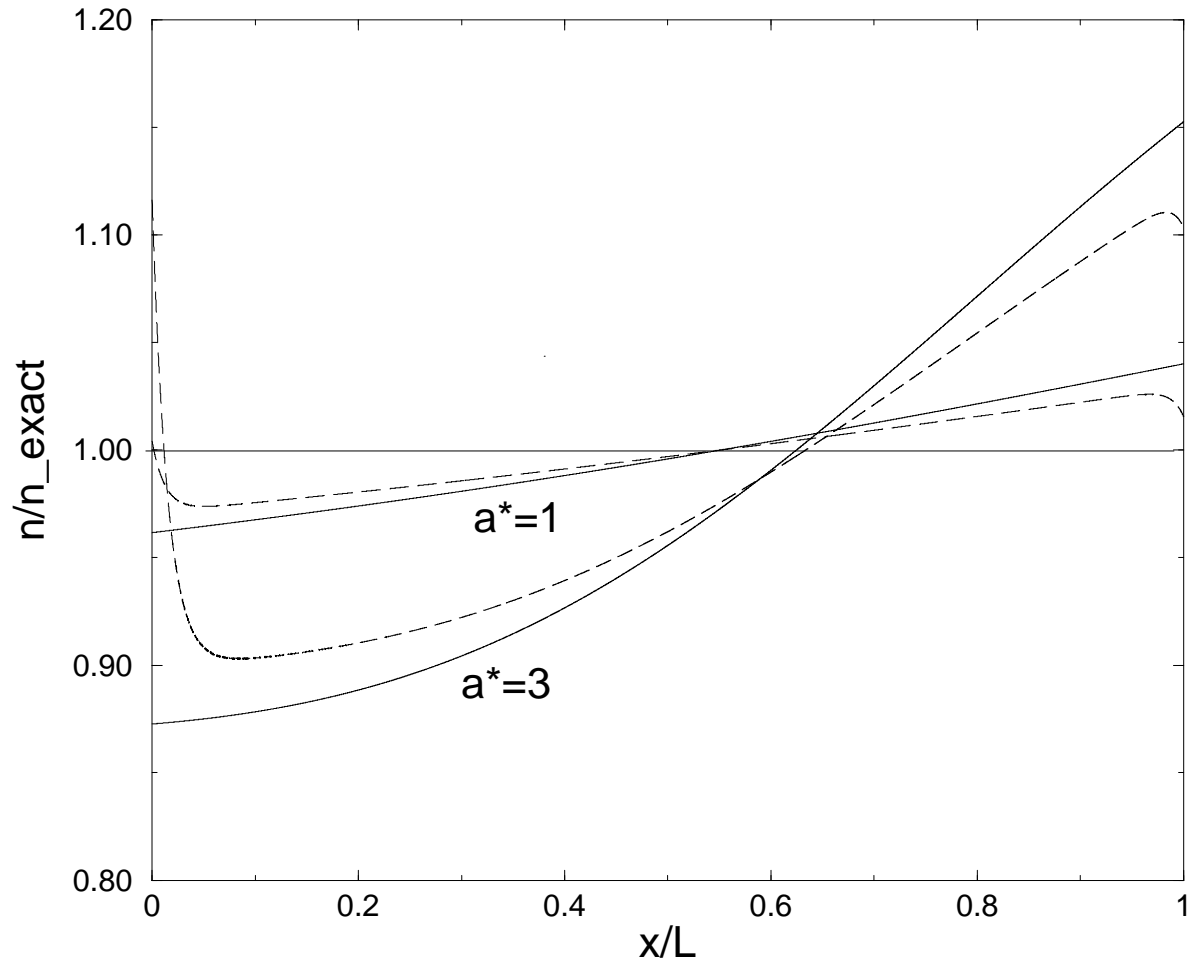


Figure 2: Reduced current J^* as a function of the reduced applied field $a^* = E/E_T$. Filled symbols correspond to the Q_3 model while open symbols to the Q_5 model. Circles, squares and diamonds correspond to $\gamma^* = 0.1, 5$ and 10 respectively. Solid, dashed and long-dashed lines are the theoretical predictions for the three values of γ^* . The horizontal line highlights the limiting plateau $J^* = 1$.

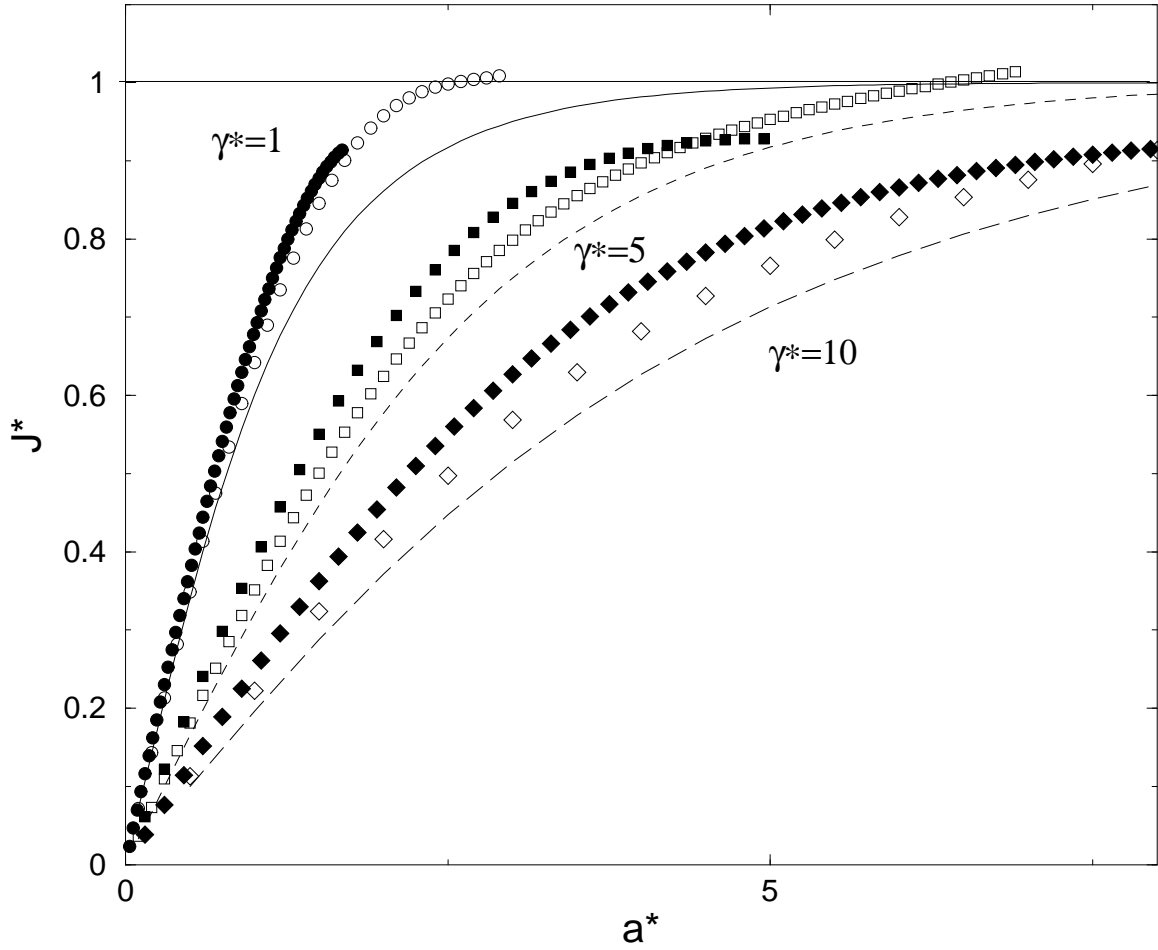


Figure 3: The pointwise error of the numerical vs. analytical solution for the density and current at the midpoint of the channel for the Q_5 lattice as a function of the number of grid points N . Circles and squares refer to density and current respectively. The main parameters are $a^* = 1$ and $\gamma^* = 10$. The dashed lines correspond to N^{-1} and $N^{-1/2}$ convergence.

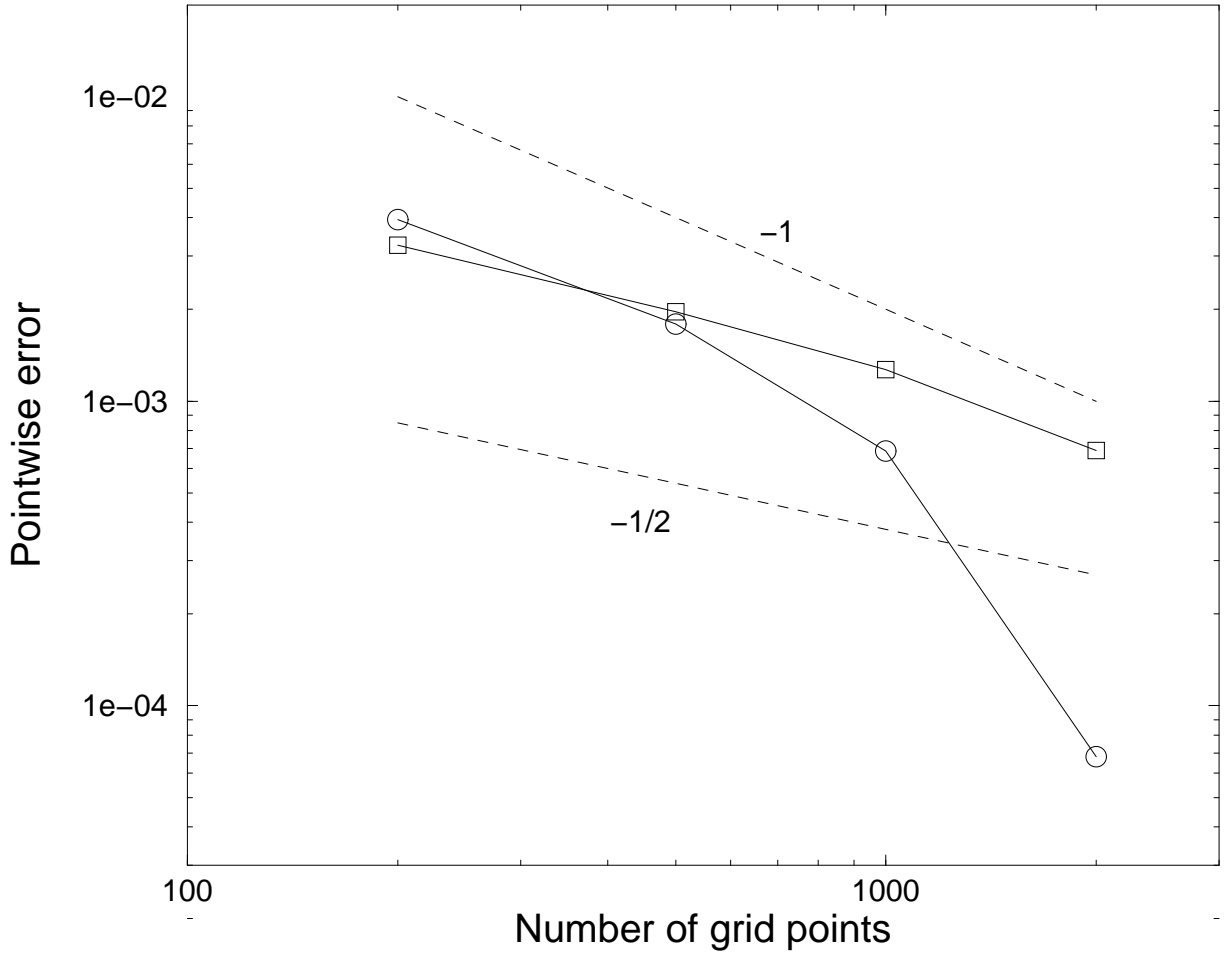


Figure 4: Ratio of currents for elastic vs. inelastic collisions, $J_{\lambda=0}/J_{\lambda=1}$, for $E_\gamma/E_T = 100$. Three values of $\lambda/\omega = 0.1, 1, \text{ and } 10$ correspond to the upper, middle and lower curves respectively. The horizontal lines represent the theoretical prediction.

